

Rigid Base Biasing in Molecular Dynamics enables enhanced sampling of DNA conformations

Aderik Voorspoels,¹ Jocelyne Vreede,² and Enrico Carlon¹

¹*Soft Matter and Biophysics, Department of Physics and Astronomy, KU Leuven*

²*Van 't Hoff Institute for Molecular Sciences, University of Amsterdam,
Science Park 904, 1098 XH Amsterdam, the Netherlands*

All-atom simulations have become increasingly popular to study conformational and dynamical properties of nucleic acids as they are accurate and provide high spatial and time resolutions. This high resolution however comes at a heavy computational cost and within the time scales of simulations nucleic acids weakly fluctuate around their ideal structure exploring a limited set of conformations. We introduce the RBB-NA algorithm which is capable of controlling rigid base parameters in all-atom simulations of Nucleic Acids. With suitable biasing potentials this algorithm can “force” a DNA or RNA molecule to assume specific values of the six rotational (tilt, roll, twist, buckle, propeller, opening) and/or the six translational parameters (shift, slide, rise, shear, stretch, stagger). The algorithm enables the use of advanced sampling techniques to probe the structure and dynamics of locally strongly deformed Nucleic Acids. We illustrate its performance showing some examples in which DNA is strongly twisted, bent or locally buckled. In these examples RBB-NA reproduces well the unconstrained simulations data and other known features of DNA mechanics, but it also allows one to explore the anharmonic behavior characterizing the mechanics of nucleic acids in the high deformation regime.

I. INTRODUCTION

All-atom molecular dynamics (MD) simulations have become standard tools to investigate the mechanical properties of DNA [1–5]. These properties are of high relevance in biological processes, as DNA is often physically deformed by proteins or other biomolecules (see Refs. [6–8] for recent reviews on DNA mechanics).

DNA force fields have been constantly improved over the years using inputs from experiments and quantum mechanical calculations [9] and simulations have reached a high degree of sophistication. At present DNA simulations have also some drawbacks. They are CPU-intensive and can thus sample molecular trajectories for only short time intervals ($\sim 1\mu s$) and short DNA sequences ($\sim 20 - 30$ base pairs). In these trajectories a DNA molecule fluctuates weakly around its ideal double helical structure. To investigate strongly deformed conformations one has to resort to advanced sampling techniques. Many enhanced sampling techniques add potentials that constrain or drive the system along a predefined collective variable. This collective variable typically involves several atoms and represents a relevant degree of freedom. In the past, umbrella sampling was used to induce strong bending by constraining the two ends of a linear DNA molecule [10]. While this approach allows one to compute the global bending free energy and to analyse kinked DNA, it provides no control at the local scale, as the bending deformation gets distributed over several base pairs. Likewise, by applying a force or a torque at the two ends one can stretch or twist a DNA molecule, but this stretching or twisting is typically distributed over all base pairs [11, 12]. On a more local scale a different advanced sampling method, metadynamics along a path in a space spanned by several coordinates representing aspects of the DNA dynamics, was used to

study Hoogsteen base pairing [13].

In this paper we introduce RBB-NA (rigid base biasing of nucleic acids), an algorithm which, by using suitable local constraints, is capable of deforming a DNA molecule by bending, stretching or twisting at the single base pair level. It enables using rigid base coordinates as the collective variable in advanced sampling techniques. Although we focus on a few illustrative examples on DNA, the algorithm also works with RNA. Different constraints can be applied simultaneously (as e.g. bend and twist) either to a single site or to multiple sites, contiguous or not, of a DNA sequence. As such, RBB-NA is a very flexible tool to investigate structure, energetics and dynamics of highly deformed DNA molecules in MD simulations. RBB-NA is available as a package in the Open Source Library PLUMED [14, 15], implemented as a collective variable. PLUMED already contains much functionality to allow advanced sampling techniques, such as metadynamics, umbrella sampling and various path sampling techniques.

II. MATERIALS AND METHODS

A. The RBB-NA algorithm

The aim of the algorithm is to compute suitable constraint forces $\vec{F}_i^{(c)}$ which act on a group of atoms (i labels a given atom) and induce different bending, twist or stretching. The flowchart shown in Fig. 1 depicts the operations of RBB-NA. It essentially consists of three different steps (labeled as 1, 2 and 3 in Fig. 1) which are schematically described in the rest of this Section.

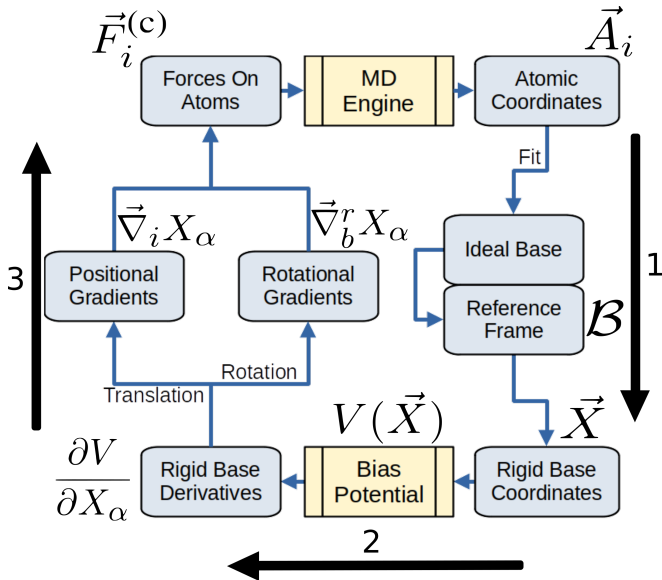


Figure 1. A flowchart showing the operations done by RBB-NA. The numbered arrows correspond to (1) Mapping onto rigid base coordinates, as done in Curves+, (2) Introducing constraints at rigid base level using the potential $V(\vec{X})$ (3) Calculating constraints forces on atoms $\vec{F}_i^{(c)}$. This third step consists of translational and rotational constraints. Total forces used in the MD integration step are the sum of constraints ($\vec{F}_i^{(c)}$) and force fields contributions ($\vec{F}_i^{(ff)}$). Constraints are typically applied to a limited set of atoms in the bases, hence the running of the algorithm does not significantly slow down the running of the MD code.

1. 1. From atomic to rigid base coordinates.

This first step performs a mapping from atomic coordinates \vec{A}_i to rigid base coordinates for the bases to which the constraint is applied. Rigid base coordinates have long been a standard description of the double helix down to the base level [16]. Software packages to extract rigid base coordinates, such as Curves+ [17] and x3dna [18], were developed in the past. Usually these packages are used in a post-processing analysis step of MD trajectories. In our algorithm we have implemented Curves+ to map atomic coordinates to rigid base coordinates during the simulation run. We briefly recall how Curves+ works. To obtain the rigid base coordinates one first associates to each base a reference frame $\mathcal{B} \equiv \{\mathbf{B}, \vec{r}\}$ consisting of an orthonormal triad of unit vectors $\mathbf{B} = [\hat{e}_1, \hat{e}_2, \hat{e}_3]$ (Fig. 2) and their origin \vec{r} . This step conventionally involves fitting a set of “ideal” base coordinates to the actual atomic coordinates measured in simulation. To parametrize the translations and rotations connecting two complementary base frames on the opposite strands of a DNA molecule one uses the rigid base coordinates \vec{d} (a vector whose components are referred to as shear, stretch and stagger in the DNA literature [16]) and $\vec{\omega}$ (buckle, propeller and opening). The coordi-

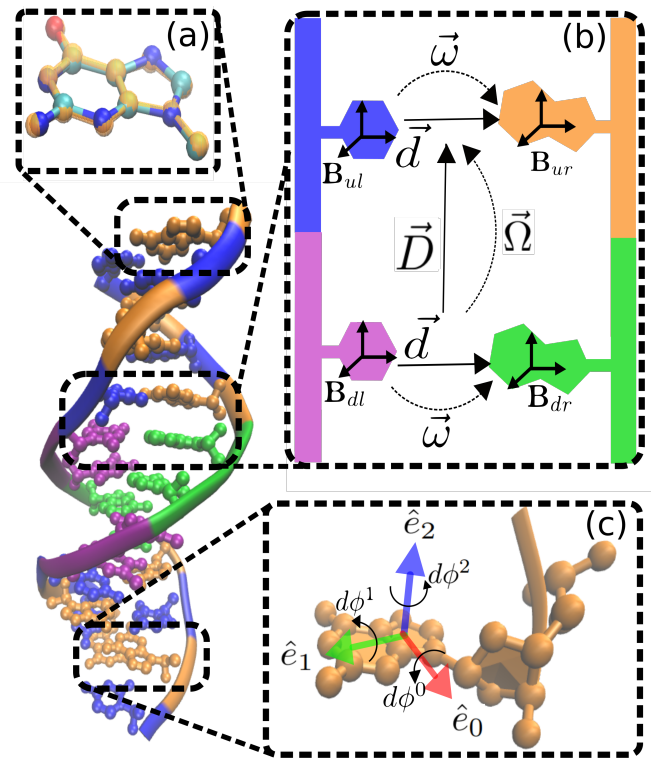


Figure 2. Illustration of different steps of the RBB-NA algorithm. (a) Mapping of atomic coordinates of a base (colored) into an ideal base configuration (orange). (b) From the reference frames $\mathcal{B} = (\mathbf{B}, \vec{r})$ consisting each of an orthonormal triad \mathbf{B} and its origin \vec{r} one calculates translational (\vec{d}, \vec{D}) and rotational ($\vec{\omega}, \vec{\Omega}$) rigid base coordinates. ($\vec{d}, \vec{\omega}$) are intra-base coordinates, while ($\vec{D}, \vec{\Omega}$) are inter-base coordinates. (c) Rigid body rotations are used to calculate the constraint forces $\vec{F}_i^{(c)}$. Steps (a) and (b) are as in the Curves+ algorithm [17].

ates \vec{D} (shift, slide and rise) and $\vec{\Omega}$ (tilt, roll and twist) parametrize translations and rotations between two consecutive base-pairs, see Fig. 2. More details are given in SI.

2. 2. The constraint potential.

For a sequence of N base pairs one has N base pair coordinates ($\vec{d}, \vec{\omega}$) and $N - 1$ base pair steps coordinates ($\vec{D}, \vec{\Omega}$). We collect all rigid base coordinates into a single $12N - 6$ dimensional vector

$$\vec{X} \equiv (\vec{\omega}_1, \vec{d}_1, \dots, \vec{\omega}_N, \vec{d}_N, \vec{\Omega}_1, \vec{D}_1, \dots, \vec{\Omega}_{N-1}, \vec{D}_{N-1}) \quad (1)$$

In principle, the constraint potential is a generic function $V(\vec{X})$ of all these coordinates. In practice, we fix constraints to a limited number of base pairs and rigid base coordinates, as shown in the examples discussed in Results.

3. 3. Translational and Rotational constraints.

In order to implement the constraints in the MD simulation one needs to compute the forces acting on each particle. The constraint force on the i -th particle is given by

$$\vec{F}_i^{(c)} = -\vec{\nabla}_i V(\vec{X}) = -\sum_{\alpha} \frac{\partial V}{\partial X_{\alpha}} \vec{\nabla}_i X_{\alpha} \quad (2)$$

where the sum runs through all $12N - 6$ components of the vector \vec{X} , α labels rigid base coordinates and $\vec{\nabla}_i$ is the gradient with respect to the cartesian coordinates of the i -th particle. The derivatives $\frac{\partial V}{\partial X_{\alpha}}$ are trivial to compute as the function $V(\vec{X})$ is analytically simple (see examples in Results). To compute $\vec{\nabla}_i X_{\alpha}$ one would need to know the function that maps atomic coordinates into rigid base coordinates \vec{X} . However, the relation between the two sets of variables is complex, in part because it makes use of fitting procedures. Unfortunately these fitting methods make the mapping between non-differentiable. Moreover, the mapping is not one-to-one, as there are multiple atomic configurations that map to the same rigid base coordinate set. The approximation made here to resolve these issues, is to treat the bases as rigid when calculating and applying constraint forces. To incorporate the entire base into the computation of \vec{X} , and to reduce noise ideal base atomic coordinates are fitted to the measured ones. Afterwards, when forces are calculated, the measured coordinates are taken to represent a rigid body.

There are two different types of rigid base coordinates: those associated to translations (\vec{d}, \vec{D}) and those associated to rotations ($\vec{\omega}, \vec{\Omega}$). The calculation of $\vec{\nabla}_i X_{\alpha}$ for translations is trivial. This is just a unit vector parallel to the component of the translation X_{α} . For rotations the construction of $\vec{\nabla}_i X_{\alpha}$ is less straightforward. It requires the computation of rotational gradients $\vec{\nabla}_b^i X_{\alpha}$ with respect to the orientation of the bases as a whole, from which torques can be calculated. Using rigid body dynamics these torques can then be converted to forces. Details of this procedure are given in SI.

Once the constraint forces $\vec{F}_i^{(c)}$ on all the atoms in the constrained bases are computed, we add to these the force fields contributions $\vec{F}_i^{(ff)}$ so the total force on the i -th atom is

$$\vec{F}_i^{\text{tot}} = \vec{F}_i^{(c)} + \vec{F}_i^{(ff)} \quad (3)$$

This is used in the MD step to update positions and velocities from the current time t to $t + \Delta t$. We note that in our scheme only atoms in bases are constrained, as these are the atoms used by Curves+ to calculate rigid base coordinates. Atoms in the backbone are not constrained.

B. Simulations

1. System Preparation.

All simulations were done using version 2020.4 of Gromacs [19], version 2.8.0 of PLUMED [14] and the Amberff99 parmbsc1 force field [9]. The RBB-NA algorithm has been implemented to work with Gromacs, however, because PLUMED is a highly portable plugin, it can be made to work with a multitude of MD engines after some minor adjustments. Water was modelled using the TIP-3P model [20], non-bonded interactions were cutoff at 1.0 nm and PME Mesh Ewald interactions was used for electrostatics. All simulations started from the structure of the Drew-Dickerson (DD) dodecamer [21], a self-complementary oligomer with sequence CGC-GAATTTCGCG which has been extensively investigated in prior experimental and computational studies (see e.g. Ref. [22]). The DD sequence was placed into a dodecahedral box, leaving 2.0 nm on either side of the molecule, with periodic boundary conditions and solvated in a 150 mM NaCl solution after which the overall charge in the system was neutralised. This structure was energy minimised with a tolerance of 1000 kJ/mol to make sure no overlap remained between solvent molecules and DNA. Subsequently, the molecule was equilibrated in the NVT ensemble for 100 ps where temperature was kept at 300 K using a velocity rescaling thermostat [23] and then equilibrated for another 100 ps in the NPT ensemble at the same temperature but using a Parrinello-Rahman barostat [24] to fix the pressure at 1.0 bar. These first equilibration simulations were performed using a 2 fs time step in a leapfrog integrator, using LINCS [25] to constrain the covalent bonds involving hydrogen atoms.

2. Production Runs.

A reference unconstrained MD simulation of 100 ns was performed with the same settings as the NPT equilibration. Snapshots were stored every 1 ps and collective variables were printed with the same frequency. Subsequently three sets of simulations were done using the RBB-NA algorithm. All three were umbrella sampling runs which will be analysed for different applications in the results section III. In the runs we used three different type of constraints induced by parabolic potentials

$$V_{\alpha} = \frac{K_{\alpha}}{2} (X_{\alpha} - \bar{X}_{\alpha})^2 \quad (4)$$

where X_{α} is either Roll, Twist or Buckle. The Roll and Twist constraints were applied on the central base pair step (AT) of the DD sequence. The Buckle constraint was applied on the second GC pair of the DD sequence. In all constrained simulations we set the spring constant to $K_{\alpha} = 1000$ kJ/mol.

For the case of the Roll simulation run the system was first pulled from its equilibrium configuration. This

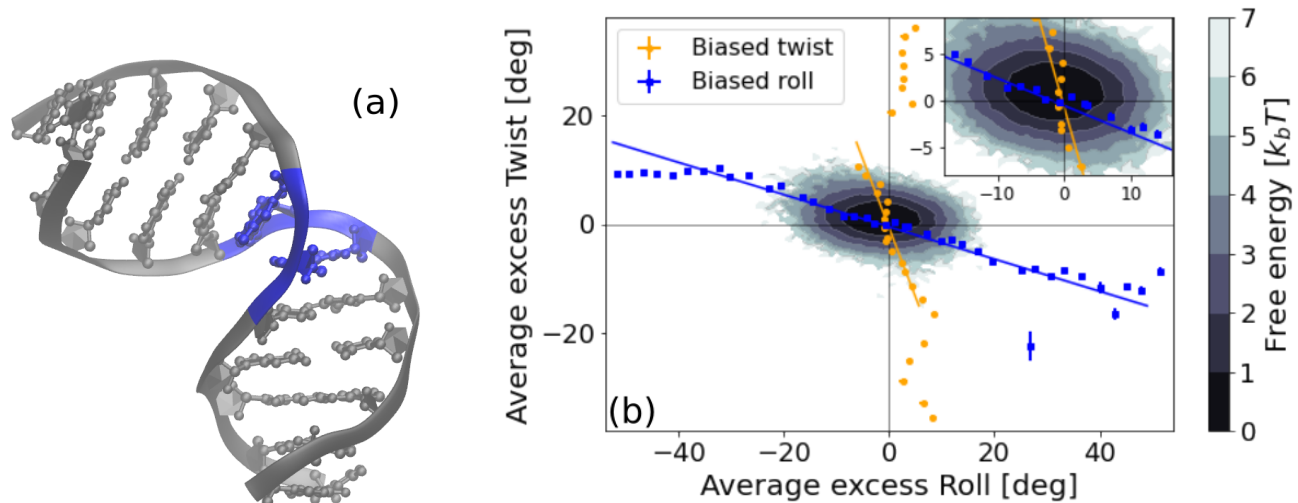


Figure 3. Simulations data obtained from the RBB-NA algorithm. (a) Snapshot of a simulation in which a local bending is imposed by a constraint on the roll Ω_2 (via Eq. (5) with $K_r = 1000$ kJ/mol and $\bar{\Omega}_2 = 1.0$ radian) in the central AT pair of the DD dodecamer. The twist-roll coupling induces a bending of the molecule. (b) Colored circles: average excess roll vs. average excess twist in simulations biasing the twist via (6) (blue circles) and the roll via Eq. (5) (orange circles). For small excess roll and twist the relation between these two variables is linear, as expected in the harmonic regime (solid lines, see SI for details). In the simulations we used $K_t = K_r = 1000$ kJ/mol. The contour plot, shown in details in the inset, is a free energy calculation from unbiased MD simulations.

was done by running molecular dynamics in consecutive 100 ps pulling windows with the same settings as the NPT equilibration but decreasing the time step to 0.2 fs. In these runs the average Roll, \bar{X}_α in the potential (4), was increased (or decreased) by 0.01 radians (starting from a zero Roll average) every pulling window. Here a maximum of 1.0 radians and a minimum of -1.0 radians were reached. The system resulting from every fifth pulling window (ie with \bar{X}_α increasing in steps of 0.05 radians) was then used to start a 10 ns production run. Here again the same settings as the NPT equilibration were used now setting the time step back to 2.0 fs. This resulted in a total of 41 windows of 10 ns with the imposed average Roll spanning from 1.0 to -1.0 radians.

After the production runs for umbrella sampling on Roll a similar procedure was carried out for Twist in the central step. Again the system was pulled from the equilibrium configuration in 100 ps windows (with the same settings as the NPT equilibration but decreasing the time step to 0.2 fs), using a potential of the shape (4), while increasing and decreasing the imposed average \bar{X}_α in steps of 0.01 radians. Notably for these Twist constraining simulation the intrinsic twist of DNA was taken into account by not starting from a zero twist average. Instead 0.61 radians was the starting average. The maximum imposed twist reached was 1.31 radians, the minimum was -0.09 radians. Like for Roll every fifth window was used to start a production run of 10 ns, with the same settings as the NPT equilibration restoring the time step to 2 fs. This resulted in 29 windows spanning an imposed average twist from -0.09 to 1.31 radians.

Finally for Buckle of the second GA pair, again the

same procedure was used. The system was pulled in 100 ps windows (with the same settings as the NPT equilibration but decreasing the time step to 0.2 fs) with the buckle changing from 0.0 radians in 0.02 radian steps. The maximum reached here was 1.3 radians, the minimum was -1.3 radians. The system resulting from every fifth pulling window (ie with the imposed average Buckle increasing in steps of 0.1 radians) was then used to start a 10 ns production run. This resulted in 17 windows.

The results in these simulations were analysed to be used in three different examples: showing coupling between Twist and roll, characterising the free energy landscape and illustrating interactions between neighboring sites in DNA.

C. Weighted Histogram Analysis

A detailed mathematical description of umbrella sampling and the Weighted Histogram Analysis Method (WHAM) that is used to reconstruct the free energy landscape has been given by J. Kaestner [26]. In short the method entails constraining the conformation space of a DNA molecule by imposing a steep potential, which is usually quadratic in the desired coordinate, as in the examples (6) and (5). By changing the location of the minimum of the constraint potential (e.g. by varying $\bar{\Omega}_3$ and $\bar{\Omega}_2$ in (6) and (5)) one can then control which region of the conformation space is sampled. If the sampled regions partially overlap, the relative free energy landscape over all regions can be reconstructed afterwards using WHAM

analysis. This involves an iterative procedure[26] which here was considered to have converged if the integral of the difference between the free energies of the previous and current iterations was below $10^{-7}k_B T$.

III. RESULTS

The RBB-NA algorithm was developed to enable umbrella sampling to characterise the free energy landscape by constraining local rigid base coordinates of DNA. However, the same algorithm can also be used in any other type of enhanced sampling applications, such as metadynamics or steered MD. We conducted three sets of umbrella sampling simulations, one imposing a local twist, one imposing a local roll and one imposing a local Buckle. From these simulations we present three different types of analysis which illustrate the functioning of the algorithm. In the first analysis, we explore how imposing a local roll or twist affects other rigid base coordinates. We find that a bias in the twist induces a non-vanishing excess roll and, vice versa, a bias in the roll induces a non-vanishing excess twist. This is a clear demonstration of the effect of twist-roll coupling [27]. In the second analysis, we compute free energy profiles along the imposed twist or roll coordinate. Here our analysis points to anharmonic behavior. Finally, the third analysis illustrates the effect of a local bias on base pairs flanking the constrained site.

A. Twist-Roll Coupling

Figure 3(a) shows a snapshot of an MD simulation in which an average excess roll of $\sim 60^\circ$ is imposed on the central base pair step (AT) of the DD sequence for which a local constraint potential of parabolic type was used

$$V_{\text{roll}} = \frac{K_r}{2} (\Omega_2 - \bar{\Omega}_2)^2 \quad (5)$$

(we use Ω_1 , Ω_2 and Ω_3 to indicate the excess tilt, roll and twist). As shown in the snapshot of Fig. 3(a) the bending induces a remarkably strong twisting deformation as well, due to the effect of the twist-roll coupling [27]. In homogeneous DNA models such interaction is described by a term of the type $G\Omega_2\Omega_3$, with G the twist-roll coupling. Twist-roll coupling and its influence on the mechanical properties of DNA has been discussed in the recent literature [28–30].

A more structured and in depth view of this coupling is given in Fig. 3(b), which shows the average excess roll vs. the average excess twist for different simulations biasing in the roll via Eq. (5), as well as for different simulations biasing in the twist, using a constraint potential of the type

$$V_{\text{twist}} = \frac{K_t}{2} (\Omega_3 - \bar{\Omega}_3)^2 \quad (6)$$

with varying values of $\bar{\Omega}_3$. This constraint imposes indeed a finite excess twist, but also a roll (Fig. 3(b)). Note that, for weak deformations, excess twist and roll induced by the biasing potentials (5) and (6) are linearly correlated. Moreover, they follow lines with different slopes (orange and blue lines in Fig. 3(b)), a behavior which can be explained by a simple harmonic model calculation, see SI. Induced excess Twist and Roll also have opposite signs, as expected for a positive twist-roll coupling $G > 0$. The contour lines in Fig. 3(b) show the free energy calculated by Boltzmann inversion ($F = -k_B T \ln(P)$, with P the equilibrium probability distribution) from the sampling of unconstrained MD simulations. The RBB-NA algorithm generates DNA conformations with roll and twist angles which greatly exceed those generated by unbiased simulations. We note that in the high deformation regime the excess twist and roll are more weakly coupled to each other than in the harmonic regime. For instance, biasing the excess twist above 20° does not produce a significant roll and a roll bias below -30° does not lead to an increase of the twist, see Fig. 3(b). While the mechanics of DNA in the weak deformations regime has been intensively studied [3, 4], the strong deformation regime is still largely unexplored. This regime is now within the reach of the RBB-NA algorithm.

B. Free energies from umbrella sampling

The tight control over rotation angles of the RBB-NA algorithm can be used for umbrella sampling to obtain free energies. Figure 4 shows a comparison between free energies obtained by unconstrained simulations (dashed lines) and with the RBB-NA algorithm via umbrella sampling (solid lines). The latter are calculated using the constraints (6) and (5). A much wider range of twist and roll angles is available via umbrella sampling. For roll, Fig. 4(a), beyond a narrow interval around the free energy minimum, the landscape no longer follows a parabolic shape. The roll data instead suggest a behavior reminiscent of the linear sub-elastic chain (LSEC) model, which was introduced to explain anomalous high bending of DNA as observed in Atomic Force Microscopy (AFM) experiments [31] (we note that AFM data analysis has led to some debate and to different conclusions about the existence of an actual anomalous bending behavior [32]). The LSEC model posits that the bending free energy of DNA is quadratic for low bending angles, while it is linear beyond a given threshold [31]. This implies that large bend angles are less costly than the quadratic model would predict. A free energy consistent with the LSEC model was also observed in prior all-atom simulations [10], where a short DNA sequence was forced to bend by applying a constraint at its two ends. Such constraint induces bending which is distributed over several nucleotides, while the RBB-NA constraint of Fig. 4 acts only on two adjacent base pairs (twist is an inter-base coordinate). The control of rigid base coordinates offered

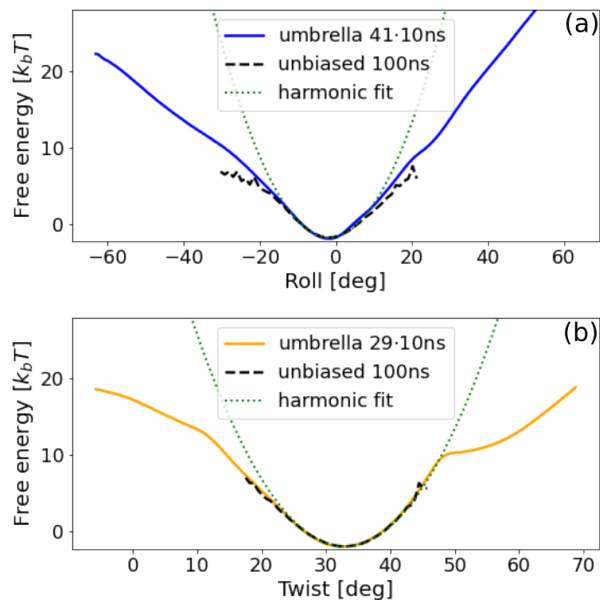


Figure 4. Free energy of roll (a) and twist (b) deformation of the central (AT) step of the DD dodecamer. Solid orange line: Umbrella sampling with the CRT-NA algorithm. Dashed lines: Sampling from unconstrained simulations. The latter can generate only small deformations around the minimal free energy state. The umbrella sampling reproduces very well the unconstrained simulations data. Dotted lines: parabolic fits to the unconstrained simulation. Both examples show deviations from the “ideal” parabolic behavior indicating that highly bent or highly twisted deformations are energetically less costly than a quadratic model would predict. Both data show asymmetries with respect to positive or negative excess roll and twist.

by the RBB-NA algorithm will hopefully provide more insights on the microscopic origin of the LSEC behavior.

The free energy landscape for twist is shown in Fig. 4(b). Again we note a good overlap between unconstrained and umbrella sampling simulations. Compared to the roll data, the twist follows a harmonic behavior for a wider range of angles. For high over and undertwisting we observe deviations from the parabolic free energy profile, which indicate that highly deformed twisted conformations are more likely than a quadratic model would predict. The deviations from the harmonic behavior are however different than in roll, showing more abrupt transitions. The overtwisted regime closely follows the quadratic shape predicted by the TWLC until a total twist of $\approx 48^\circ$ is reached. There, the landscape shows a sharp transition which, upon close inspection of the trajectories, can be linked to a structural change involving partial breaking of the hydrogen bonds. In the undertwisted regime one can also note an abrupt change of behavior in the free energy around a total twist of 15° , although less sharp than in the overtwisted case. We note that here we have sampled free energies for roll and twist as induced by biasing via Eqs. (6) and (5). This analysis

provides just a “one-dimensional” projection of the two dimensional free energy $f(\Omega_2, \Omega_3)$. The full calculation of this free energy will be presented elsewhere.

C. Effect of a local bias on neighboring sites

Several studies have observed correlations between rigid base coordinates separated by a few nucleotides along the sequence, indicating the existence of couplings between distal sites [1, 2, 33]. A recent analysis quantified these non-local couplings for tilt, roll and twist both for DNA [34] and dsRNA [35]. Very similar couplings were found in these two molecules [35]. Here we analyze structural deformations along the whole sequence of a DD dodecamer induced by local perturbations at a specific site.

Figure 5(a) shows the average excess twist in the DD sequence upon imposing an excess twist via a potential of the type (6) on the central AT site, with the different lines referring to different strengths of the perturbation. We note that the perturbation produces an oscillating decay of the twist. This is in line with the predictions of non-local models of DNA and dsRNA elasticity [34, 35]. This behavior can be understood by a minimal (homogenous) model of twist free energy E_{twist} of the following type

$$E_{\text{twist}} = \frac{1}{2} \sum_n \left[\tilde{C} \Omega_3^2(n) + \tilde{C}' \Omega_3(n) \Omega_3(n+1) \right] \quad (7)$$

where the sum runs through all the sites and \tilde{C} and \tilde{C}' are the on-site and next-neighbor torsional stiffnesses and $\Omega_3(n)$ is the excess twist at site n . For simplicity we have limited the off-site interactions to a coupling between consecutive sites n and $n \pm 1$, but this argument can be easily extended to interactions coupling more distant sites, as n and $n + 2$ etc. . . [34]. Prior work showed that both DNA and dsRNA are characterized by $\tilde{C}' > 0$ [35], while stability requires that $\tilde{C} > 0$. Let us consider a perturbation of type (6) enforcing $\langle \Omega_3(k) \rangle > 0$ at a given site k . As $\tilde{C}' > 0$ energy minimization induces $\langle \Omega_3(k \pm 1) \rangle < 0$ at the two flanking sites. This ultimately produces an alternating decaying profile of over- and undertwist.

Finally, we used RBB-NA to induce a buckle (ω_1) which is an intra base-pair parameter describing the mutual orientation of two complementary bases in the same pair. Buckle is the angle formed by a rotation around the pair short axis. A non-zero buckle was induced using the following constraint

$$V_{\text{buckle}} = \frac{K}{2} (\omega_1 - \bar{\omega}_1)^2 \quad (8)$$

Instead of an alternating pattern buckle shows a monotonic decay, see Fig. 5(b). This type of behavior can be generated by a buckle free energy of the same form as Eq. (7), but with a negative off-site stiffness (corresponding to $\tilde{C}' < 0$). We note that the decay of the buckle is asymmetric, which may be due to sequence or end effects.

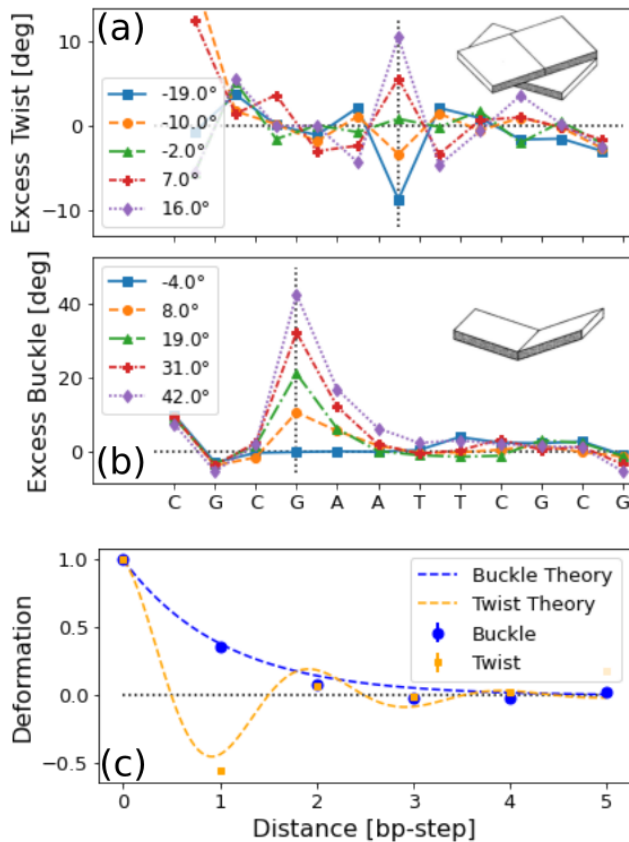


Figure 5. (a) Average excess twist induced along the molecule by a twist deformation imposed by a constraint of type (6) in the central AT step of the DD dodecamer. The twist has an oscillatory decay as predicted by a twist free energy of type (7) with $\tilde{C}' > 0$. Note that Curves+ reports an anomalous high twist at the left end of the sequence, presumably due to some end effects. (b) Average excess buckle induced by a constraint of type (8) applied to the second G nucleotide from the left. (c) Average decays of twist and buckle from MD simulations (symbols) and predictions from continuum non-local Twistable Wormlike chain model [34, 35].

Figure 5(c) compares the results of simulations directly to the theory of non-local DNA elasticity developed in [34]. For twist, good agreement is found between the observed oscillatory decay and theoretical predictions (dashed lines). Buckle, which was not included in previous studies, also decays exponentially along the chain as a result of a local perturbation, a clear signature of an off-site (non local) coupling. Parameters needed to determine the theoretical decay profile, local stiffness and off site couplings, were determined using the same reference simulation used in the umbrella sampling simulations.

IV. DISCUSSION

We have developed an algorithm (RBB-NA) which allows one to control rigid base parameters in DNA. In

RBB-NA suitable bias potentials are used to impose specific values to one (or more than one) of the twelve rigid base parameters tilt, roll, twist, buckle, propeller, opening, shift, slide, rise, shear, stretch and stagger. The algorithm uses rigid body dynamics to translate potentials on complex collective variables into constraining forces which act on atoms during simulations. RBB-NA can thus generate highly deformed DNA in a controlled manner at the local scale, e.g. at the base pair level. We believe that the algorithm offers an interesting new tool to explore the dynamics of rare events and to map the full free energy landscape, by using advanced sampling techniques, well-beyond what unconstrained simulations can reach.

After giving a schematic overview of the working of RBB-NA (see SI for more mathematical details), we have discussed three examples. The first one shows how a bias in the twist actually induces an excess roll as well, and vice-versa, a bias in the roll induces a non-zero excess twist. This is an illustration of the twist-roll coupling. Although this coupling is well-known in DNA [27] and also studied at length in the recent literature [28–30], the fact that we can observe its effect in RBB-NA is an indication that the algorithm works correctly. We find indeed that a positive excess twist bias induces a negative roll and vice-versa, as expected in the case of positive twist-roll coupling constant $G > 0$, in agreement with prior studies [16]. Apparent from these results is also the opportunity RBB-NA provides to study the structure of highly deformed conformations of DNA, such as the snapshot shown in Fig. 3(a). Correspondingly one can see from Fig. 3(b), comparing the area accessible in unconstrained sampling to the reach of the simulations using RBB-NA, the breadth of conformations which can now be accessed in a highly controlled manner.

The second example shows free energy calculations where RBB-NA was used to perform umbrella sampling simulations. We considered again roll and twist deformations as illustrative. The results of these simulations were analyzed using WHAM. Notable here is that this relatively straightforward application of the algorithm already reveals some interesting features in the presented free energy landscape. Especially interesting is the LSEC behaviour of Roll. This result is in line with previous experimental [31] and computational [10] findings. Here, however, we can for the first time attribute, the previously observed behaviour, to the local basepair step scale. As such RBB-NA is a promising tool that could be used in future studies to uncover the precise origin of this anharmonic behaviour. Moreover RBB-NA can be used in umbrella sampling studies to identify other relevant and interesting features in the free energy landscape of dsDNA like was done for twist. While here only “one-dimensional” projections of the entire free energy landscape have been discussed. RBB-NA might well be used to explore and map the full 12 dimensional free energy landscape or other interesting subsets thereof. This complete free energy landscape is likely to hold features

(barriers, dips, local minima, ...) which are important for the biological functioning of DNA.

Finally, in a third example we investigated how a local perturbation propagates to neighboring sites. Here results were presented for twist and buckling deformations which show two different types of spatial propagation: twist decays through damped oscillations, while buckle shows a monotonic decay. This behavior can be attributed to the different signs of the non-local coupling terms, as discussed in [34].

We believe that the possibility of deforming DNA (or RNA) at the local scale will provide several new insights on the structural and dynamical properties of Nucleic Acids. In addition, the possibilities of computing free

energies in the high deformation regime, beyond the harmonic regime will lead to an improved parametrization of rigid base coarse-grained models of DNA [5, 36].

A. Availability

The RBB-NA code is made available through github: <https://github.com/AderikVoorspoels/RBB-NA.git>.

ACKNOWLEDGEMENTS

We acknowledge interesting discussions with Midas Segers and Enrico Skoruppa.

-
- [1] F. Lankaš, J. Šponer, J. Langowski, and T. E. Cheatham, DNA basepair step deformability inferred from molecular dynamics simulations, *Biophys. J.* **85**, 2872 (2003).
- [2] A. Noy and R. Golestanian, Length scale dependence of DNA mechanical properties, *Phys. Rev. Lett.* **109**, 228101 (2012).
- [3] M. Pasi, J. H. Maddocks, D. Beveridge, T. C. Bishop, D. A. Case, T. Cheatham, P. D. Dans, B. Jayaram, F. Lankaš, C. Laughton, J. Mitchell, R. Osman, M. Orozco, A. Pérez, D. Petkevičiute, N. Spackova, J. Sponer, K. Zakrzewska, and R. Lavery, μ ABC: A systematic microsecond molecular dynamics study of tetranucleotide sequence effects in B-DNA, *Nucl. Acids Res.* **42**, 12272 (2014).
- [4] V. Velasco-Berrelleza, M. Burman, J. W. Shepherd, M. C. Leake, R. Golestanian, and A. Noy, SerraNA: a program to determine nucleic acids elasticity from simulation data, *Phys. Chem. Chem. Phys.* **22**, 19254 (2020).
- [5] J. Walther, P. D. Dans, A. Balaceanu, A. Hospital, G. Bayarri, and M. Orozco, A multi-modal coarse grained model of DNA flexibility mappable to the atomistic level, *Nucl. Acids Res.* **48**, e29 (2020).
- [6] A. Aggarwal, S. Naskar, A. K. Sahoo, S. Mogurampelly, A. Garai, and P. K. Maiti, What do we know about DNA mechanics so far?, *Curr. Op. Struct. Biol.* **64**, 42 (2020).
- [7] H. Dohnalová and F. Lankaš, Deciphering the mechanical properties of B-DNA duplex, *WIREs Comput. Mol. Sci.* **12**, e1575 (2021).
- [8] A. Marin-Gonzalez, J. Vilhena, R. Perez, and F. Moreno-Herrero, A molecular view of DNA flexibility, *Q. Rev. Biophys.* **54**, 10.1017/S0033583521000068 (2021).
- [9] I. Ivani, P. Dans, A. Noy, A. Pérez, I. Faustino, A. Hospital, J. Walther, P. Andrio, R. Goñi, A. Balaceanu, G. Portella, F. Battistini, J. Gelpí, C. González, M. Vendruscolo, C. Laughton, S. Harris, D. Case, and M. Orozco, Parmbsc1: a refined force field for DNA simulations, *Nat. Methods* **13**, 55 (2016).
- [10] J. Curuksu, M. Zacharias, R. Lavery, and K. Zakrzewska, Local and global effects of strong dna bending induced during molecular dynamics simulations, *Nucl. Acids Res.* **37**, 3766 (2009).
- [11] A. Marin-Gonzalez, J. Vilhena, R. Perez, and F. Moreno-Herrero, Understanding the mechanical response of double-stranded DNA and RNA under constant stretching forces using all-atom molecular dynamics, *Proc. Natl. Acad. Sci.* **114**, 7049 (2017).
- [12] J. W. Shepherd and M. C. Leake, The end restraint method for mechanically perturbing nucleic acids in silico, in *Chromosome Architecture* (Springer, 2022) pp. 249–262.
- [13] A. Pérez de Alba Ortíz, J. Vreede, and B. Ensing, Sequence dependence of transient hoogsteen base pairing in dna, *PLoS computational biology* **18**, e1010113 (2022).
- [14] G. A. Tribello, M. Bonomi, D. Branduardi, C. Camilloni, and G. Bussi, PLUMED 2: New feathers for an old bird, *Computer physics communications* **185**, 604 (2014).
- [15] The PLUMED consortium, Promoting transparency and reproducibility in enhanced molecular simulations, *Nature Methods* **16**, 670 (2019).
- [16] W. K. Olson, M. Bansal, S. K. Burley, R. E. Dickerson, M. Gerstein, S. C. Harvey, U. Heinemann, X. J. Lu, S. Neidle, Z. Shakked, H. Sklenar, M. Suzuki, C. S. Tung, E. Westhof, C. Wolberger, and H. M. Berman, A standard reference frame for the description of nucleic acid base-pair geometry, *J. Mol. Biol.* **313**, 229 (2001).
- [17] R. Lavery, M. Moakher, J. Maddocks, D. Petkevičiute, and D. Zakrzewska, Conformational analysis of nucleic acids revisited: Curves+, *Nucl. Acids Res.* **37**, 5917–5929 (2009).
- [18] S. Li, W. Olson, and X.-J. Lu, Web 3DNA 2.0 for the analysis, visualisation, and modelling of 3D nucleic acid structures, *Nucl. Acids Res.* **47**, W26 (2019).
- [19] M. Abrahams, T. Murtola, R. Schulz, S. Páll, J. Smith, B. Hess, and E. Lindahl, GROMACS: high performance molecular simulations through multi-level parallelism from laptops to supercomputers, *SoftwareX* **1-2**, 19 (2015).
- [20] W. L. Jorgensen, J. Chandrasekhar, J. D. Madura, R. W. Impey, and M. L. Klein, Comparison of simple potential functions for simulating liquid water, *J. Chem. Phys.* **79**, 926 (1983).
- [21] R. Dickerson, Definitions and nomenclature of nucleic acid structure components, *Nucl. Acids Res.* **17**, 1797 (1989).
- [22] T. Drsata, A. Pérez, M. Orozco, A. V. Morozov, J. Sponer, and F. Lankaš, Structure, stiffness and

- substates of the Dickerson-Drew dodecamer, *J. Chem. Theor. Comp.* **9**, 707 (2013).
- [23] G. Bussi, D. Donadio, and M. Parrinello, Canonical Sampling Through Velocity Rescaling, *J. Chem. Phys.* **126**, 014101 (2007).
- [24] M. Parrinello and A. Rahman, Polymorphic transitions in single crystals: A new molecular dynamics method, *J. Appl. Phys.* **52**, 7182 (1981).
- [25] B. Hess, H. Bekker, H. J. C. Berendsen, and J. G. E. M. Fraaije, LINCS: A linear constraint solver for molecular simulations, *J. Comput. Chem.* **18**, 1463 (1997).
- [26] J. Kaestner, Umbrella sampling, *Wiley interdisciplinary reviews. Computational molecular science* **1**, 932 (2011).
- [27] J. Marko and E. Siggia, Bending and twisting elasticity of DNA, *Macromolecules* **27**, 981 (1994).
- [28] E. Skoruppa, S. Nomidis, J. F. Marko, and E. Carlon, Bend-Induced Twist Waves and the Structure of Nucleosomal DNA, *Phys. Rev. Lett.* **121**, 088101 (2018).
- [29] M. Caraglio, E. Skoruppa, and E. Carlon, Overtwisting induces polygonal shapes in bent DNA, *J. Chem. Phys.* **150**, 135101 (2019).
- [30] S. K. Nomidis, M. Caraglio, M. Laleman, K. Phillips, E. Skoruppa, and E. Carlon, Twist-bend coupling, twist waves, and the shape of DNA loops, *Phys. Rev. E* **100**, 022402 (2019).
- [31] P. A. Wiggins, D. H. Van, F. Moreno-herrero, A. Spakowitz, R. Phillips, J. Widom, C. Dekker, and P. C. Nelson, High flexibility of DNA on short length scales probed by atomic force microscopy, *Nature Nanotechnology* **1**, 137 (2006).
- [32] A. K. Mazur and M. Maaloum, Atomic force microscopy study of DNA flexibility on short length scales: smooth bending versus kinking, *Nucl. Acids Res.* **42**, 14006 (2014).
- [33] B. Eslami-Mossallam and M. Ejtehadi, Contribution of nonlocal interactions to DNA elasticity, *J. Chem. Phys.* **134**, 03B623 (2011).
- [34] E. Skoruppa, A. Voorspoels, J. Vreede, and E. Carlon, Length-scale-dependent elasticity in DNA from coarse-grained and all-atom models, *Phys. Rev. E* **103**, 042408 (2021).
- [35] M. Segers, A. Voorspoels, T. Sakaue, and E. Carlon, Mechanical properties of nucleic acids and the non-local twistable wormlike chain model, *J. Chem. Phys.* **156**, 234105 (2022).
- [36] M. Orozco, A. Noy, and A. Pérez, Recent advances in the study of nucleic acid flexibility by molecular dynamics, *Curr. Op. Struct. Biol.* **18**, 185 (2008).
- [37] A. D. McLachlan, Gene duplications in the structural evolution of chymotrypsin, *J. Mol. Biol.* **128**, 49 (1979).

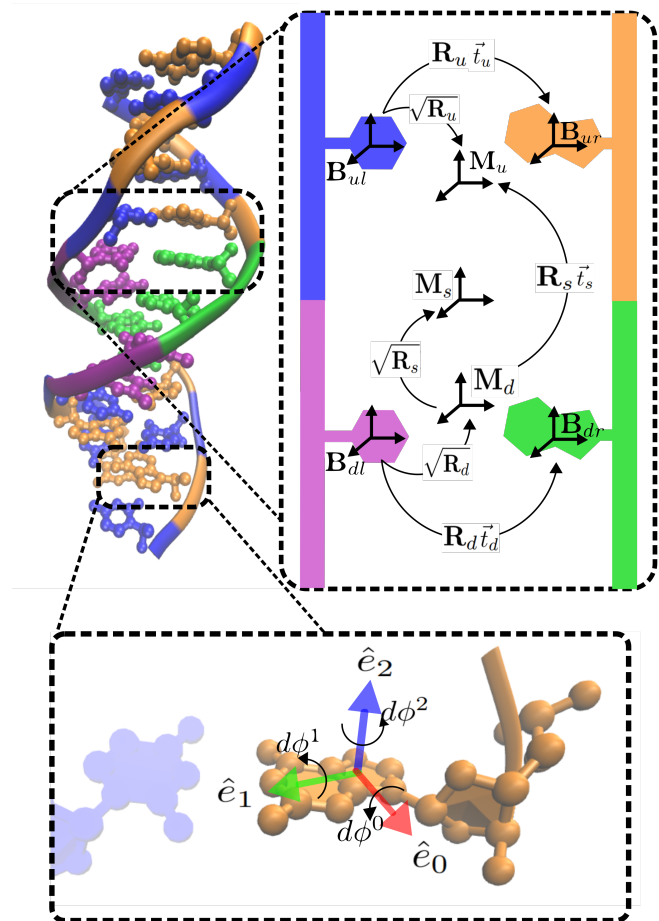


Figure S1. A strand of DNA. Attached to the right is a diagram showing the relation between different rotations and reference triad. Attached below is an illustration of the unit vectors forming a base triad and the action small rotations have on them

SUPPLEMENTAL INFORMATION

S1. MATHEMATICAL DERIVATIONS IN THE ALGORITHM

The purpose of the RBB-NA algorithm is to bias the rotational and translational rigid base coordinates \vec{X} of a DNA (or RNA) strand, given the representation of this strand as a series of bases \mathcal{B}_b . Here b ranges from 0 to $2N$ with N being the length of the strand in question in base pairs. Notably any base will during the simulation be represented by a collection of atom positions $\{\vec{A}_i\}$. It is from these atom positions that the calculation of the collective variables must start, and it is on these atoms that in the end forces can be applied using Eq. (2). For sake of completeness and to introduce the required notations and concepts this section begins with a description of the curves algorithm developed by Lavery et al. [17] which is used to calculate the collective variables. This algorithm has been re-implemented in RBB-NA to fit with

the PLUMED code base.

A. Curves in brief

The standard choice in the Curves+ software is to first fit a set of ideal base coordinates $\{\vec{A}_i^*\}$ to the measured ones by finding the appropriate rotation in a procedure described by McLachlan [37]. This is usually done to reduce the influence of fluctuations within a base on the collective variables, thus reducing the noise. For the purposes of this work this step is useful as it incorporates all heavy atoms in a given base into the calculations of the collective variables. As such it is this step that facilitates both treating the entire base as a rigid body as well as preventing forces from interfering with fluctuations in the bases themselves.

After the optional fitting the curves algorithm starts by defining reference frames \mathcal{B}_b for each base consisting of a triad of orthonormal vectors \mathbf{B}_b and a reference point \vec{r}_b where this frame is to be attached [17]. Here \mathbf{B}_b can be seen as a rotation matrix

$$\mathbf{B}_b = [\hat{e}_1, \hat{e}_2, \hat{e}_3]. \quad (\text{S1})$$

where the vectors $\hat{e}_1, \hat{e}_2, \hat{e}_3$ collectively form the base triad with \hat{e}_1 pointing into the major groove, \hat{e}_2 connecting the backbones and \hat{e}_3 being normal to the base plane.

To keep track of the different frames and many variables needed in the calculations that follow we include here a diagram (S1). On this diagram the reference frames involved in the calculation of rigid base coordinates in this particular step are labelled according to their position in relation to the step. We denote all frames in the upward direction from the step with a subscript ‘u’, The frames in the downward direction are denoted similarly with subscript ‘d’. For frames on the left strand we add ‘l’ and for those on the right ‘r’.

When the frames are constructed one defines the transformation from one base to the opposing one, say in the diagram, (S1) from \mathcal{B}_{ul} to \mathcal{B}_{ur} , by rotation matrix \mathbf{R}_u and translation \vec{t}_u which are defined as

$$\mathbf{R}_u = \mathbf{B}_{ur} \mathbf{B}_{ul}^T, \quad \vec{t}_u = \vec{r}_{ur} - \vec{r}_{ul}. \quad (\text{S2})$$

In addition to these transformations a frame in which to express them is needed. This is given by the midframe \mathcal{M}_u of this particular base pair for which the triad can be written as

$$\mathbf{M}_u = \sqrt{\mathbf{R}_u} \mathbf{B}_{ul} = \sqrt{\mathbf{R}_u^T} \mathbf{B}_{ur}. \quad (\text{S3})$$

Here the square-root $\sqrt{\mathbf{R}}$ is a short notation for $\exp \frac{1}{2} \log \mathbf{R}$ which yields a rotation about the same axis by half the angle.

In practice the midframe is not found by explicit calculation of the square root but simply by rotating the

three vectors in \mathbf{B}_{ul} around the axis of rotation of \mathbf{R}_u by half its rotation angle. For any rotation matrix the angle of rotation $\Theta(\mathbf{R})$ can be found by

$$\Theta(\mathbf{R}) = \arccos \frac{1}{2} (\text{Tr}(\mathbf{R}) - 1), \quad (\text{S4})$$

and subsequently the axis of rotation $\hat{K}(\mathbf{R})$ is given as

$$\hat{K}(\mathbf{R}) = \frac{1}{2 \sin \Theta(\mathbf{R})} \begin{bmatrix} R_{23} - R_{32} \\ R_{31} - R_{13} \\ R_{12} - R_{21} \end{bmatrix}. \quad (\text{S5})$$

This conversion of rotation matrices to axis angle representation also allows us to define the rotational collective variables of a base pair as

$$\vec{\omega}_u^T = \Theta(\mathbf{R}_u) (\hat{K}(\mathbf{R}_u))^T \cdot \mathbf{M}_u. \quad (\text{S6})$$

Similarly the translational collective variables of the basepair are defined by

$$\vec{d}_u^T = \vec{t}_u^T \cdot \mathbf{M}_u. \quad (\text{S7})$$

After the calculation of the basepair collective variables the algorithm largely repeats itself. The transformation from one pair to the next, say from \mathcal{M}_d to \mathcal{M}_u on the diagram, is now given by a rotation \mathbf{R}_s and a translation \vec{t}_s which are defined by

$$\mathbf{R}_s = \mathbf{M}_u \mathbf{M}_d^T, \quad \vec{t}_s = \frac{1}{2} (\vec{r}_{ur} + \vec{r}_{ul}) - \frac{1}{2} (\vec{r}_{dr} + \vec{r}_{dl}). \quad (\text{S8})$$

Like before a midframe is then defined by half rotation:

$$\mathbf{M}_s = \sqrt{\mathbf{R}_s} \mathbf{M}_d = \sqrt{\mathbf{R}_s^T} \mathbf{M}_u, \quad (\text{S9})$$

and finally the transformations are expressed in this midframe

$$\vec{\Omega}_u^T = \Theta(\mathbf{R}_s) (\hat{K}(\mathbf{R}_s))^T \cdot \mathbf{M}_s \quad (\text{S10})$$

$$\vec{D}_s^T = \vec{t}_s^T \cdot \mathbf{M}_s. \quad (\text{S11})$$

With these four sets of collective variables we can turn to the calculation of forces, which as noted in the main text, requires the calculation of gradients with respect to the cartesian coordinates of atom positions.

B. Calculus of rotations

The calculated rigid base-pair coordinates fall into two different categories: translations and rotations. For the two sets of translations derivation and thus the application of forces is simple, the two sets of rotations require more work. Here the construction of gradients of those two sets of rotations $\vec{\Omega}$ and $\vec{\omega}$ to small rotations of the underlying base frames $d\vec{\phi}_b$ is discussed.

To start, the derivative of the base reference frame \mathbf{B}_b to rotations $d\vec{\phi}^b$ about its own axis can be found as follows. Subsequently imposing the infinitesimal rotations $d\phi_b^0, d\phi_b^1, d\phi_b^2$ on \mathbf{B}_b yields

$$\mathbf{B}_b + d\mathbf{B}_b = \mathbf{B}_b \circ \begin{pmatrix} 1 & -d\phi^3 & d\phi^2 \\ d\phi^3 & 1 & -d\phi^1 \\ -d\phi^2 & d\phi^1 & 1 \end{pmatrix}$$

Which implies the derivative of \mathbf{B}^b is given by

$$\frac{d\mathbf{B}_b}{d\vec{\phi}_b} = \mathbf{B}_b \vec{\mathbf{S}}. \quad (\text{S12})$$

Where $\vec{\mathbf{S}}$ is a vector of skew matrices defined by

$$\vec{\mathbf{S}} = \left[\begin{pmatrix} 0 & 0 & 0 \\ 0 & 0 & -1 \\ 0 & 1 & 0 \end{pmatrix}, \begin{pmatrix} 0 & 0 & 1 \\ 0 & 0 & 0 \\ -1 & 0 & 0 \end{pmatrix}, \begin{pmatrix} 0 & -1 & 0 \\ 1 & 0 & 0 \\ 0 & 0 & 0 \end{pmatrix} \right]^T.$$

From this result the derivatives of the other relevant rotation matrices used above can be calculated. To start the derivatives of the \mathbf{R}^u are given by:

$$\frac{\partial \mathbf{R}_u}{\partial \vec{\phi}_{ul}} = \mathbf{B}_{ur} \vec{\mathbf{S}}^T \mathbf{B}_{ul}^T, \quad \frac{\partial \mathbf{R}_u}{\partial \vec{\phi}_{ur}} = \mathbf{B}_{ur} \vec{\mathbf{S}} \mathbf{B}_{ul}^T. \quad (\text{S13})$$

For the mid-pair frame \mathbf{M}_u we find:

$$\frac{\partial \mathbf{M}_u}{\partial \vec{\phi}_{ur}} = \frac{\partial \sqrt{\mathbf{R}_u}}{\partial \vec{\phi}_{ur}} \mathbf{B}_{ul} = \frac{1}{2} \sqrt{\mathbf{R}_u} \mathbf{R}_u^T \frac{\partial \mathbf{R}_u}{\partial \vec{\phi}_{ur}} \mathbf{B}_{ul} = \frac{1}{2} \mathbf{M}_u \vec{\mathbf{S}}, \quad (\text{S14})$$

and likewise:

$$\frac{\partial \mathbf{M}_u}{\partial \vec{\phi}_{ul}} = \frac{1}{2} \mathbf{M}_u \vec{\mathbf{S}}. \quad (\text{S15})$$

Where we used the fact that \mathbf{R}_u , $\sqrt{\mathbf{R}_u}$, \mathbf{R}_u^T , and $\sqrt{\mathbf{R}_u^T}$ all commute and we used both representations of the mid-frame in Eq. (S3). Similar results can be obtained for the lower basepair in a given base-pair step. As such the derivatives of the rotation matrices \mathbf{R}_s and \mathbf{M}_s relevant for the step parameters can also be written down. Doing this gives for the rotation:

$$\frac{\partial \mathbf{R}_s}{\partial \vec{\phi}_{ul}} = \frac{\partial \mathbf{R}_s}{\partial \vec{\phi}_{ur}} = \frac{1}{2} \mathbf{M}_u \vec{\mathbf{S}} \mathbf{M}_d^T, \quad (\text{S16})$$

$$\frac{\partial \mathbf{R}_s}{\partial \vec{\phi}_{dl}} = \frac{\partial \mathbf{R}_s}{\partial \vec{\phi}_{dr}} = \frac{1}{2} \mathbf{M}_u \vec{\mathbf{S}}^T \mathbf{M}_d^T. \quad (\text{S17})$$

where it should be noted derivatives to both base in the same pair have become equal. Likewise for the midframe of the step we find:

$$\frac{\partial \mathbf{M}_s}{\partial \vec{\phi}_{ul}} = \frac{\partial \mathbf{M}_s}{\partial \vec{\phi}_{ur}} = \frac{\partial \mathbf{M}_s}{\partial \vec{\phi}_{dl}} = \frac{\partial \mathbf{M}_s}{\partial \vec{\phi}_{dr}} = \frac{1}{4} \mathbf{M}_s \vec{\mathbf{S}}. \quad (\text{S18})$$

Now we have calculated the derivatives of all rotation matrices and \mathbf{R} and mid frames \mathbf{M} to small rotations of the

bases. Subsequently we need to compute the derivatives of axis angle coordinates to the corresponding rotation matrix \mathbf{R} . To do this one can simply refer to the formulas to construct the axis angle representation from a matrix in (S4) and (S5), and derive them:

$$\frac{\partial \Theta(\mathbf{R})}{\partial \mathbf{R}} = \frac{-1}{2 \sin \Theta(\mathbf{R})} \mathbf{I}_{3 \times 3}, \quad (\text{S19})$$

$$\frac{\partial \hat{K}(\mathbf{R})}{\partial \mathbf{R}} = \frac{\vec{\mathbf{S}} - \cot \Theta(\mathbf{R}) \hat{K}(\mathbf{R}) \otimes \mathbf{I}_{3 \times 3}}{2 \sin \Theta(\mathbf{R})}. \quad (\text{S20})$$

With this final bit of information the derivative of any one of our angular coordinates to a small rotation of a base frame can be written. To do this one needs only the relevant formula (S10) and the equations derived in this section. For example deriving some step rotation α to a rotation of base b about axis k would read:

$$\begin{aligned} \frac{\partial \Omega_s^\alpha}{\partial \phi_b^k} &= \frac{\partial \Theta_s}{\partial \phi_b^k} \left[\hat{K}_s \cdot \mathbf{M}_s[\alpha] \right] \\ &+ \Theta_s \left[\frac{\partial \hat{K}_s}{\partial \phi_b^k} \cdot \mathbf{M}_s[\alpha] + \hat{K}_s \cdot \frac{\partial \mathbf{M}_s[\alpha]}{\partial \phi_b^k} \right]. \end{aligned} \quad (\text{S21})$$

Here we dropped the explicit indication that Θ_s and \hat{K}_s are functions of \mathbf{R}_s . Their derivatives are calculated using the chain rule:

$$\frac{\partial \Theta_s}{\partial \phi_b^k} = \frac{\partial \Theta_s}{\partial \mathbf{R}_s} \frac{\partial \mathbf{R}_s}{\partial \phi_b^k}, \quad \frac{\partial \hat{K}_s}{\partial \phi_b^k} = \frac{\partial \hat{K}_s}{\partial \mathbf{R}_s} \frac{\partial \mathbf{R}_s}{\partial \phi_b^k}. \quad (\text{S22})$$

Subsequently these derivatives can be combined into the gradient of a rotational rigid base coordinate to the orientation of an underlying base by:

$$\vec{\nabla}_b^r \Omega_s^\alpha = \sum_k \frac{\partial \Omega_s^\alpha}{\partial \phi_b^k} \mathbf{B}_b[k]. \quad (\text{S23})$$

Note that replacing Ω by ω and s by p in the previous three equations would yield the equivalent formulas for a pair rotation.

C. Rigid body dynamics

Having calculated the gradients of the desired collective variables, we can recall Eq. (2). While the precise gradients to atomic positions \vec{A}_i are not known, and thus we can not write out equations for the atomic forces, the rotational gradients to small rotations of the bases are known. Considering the bases as rigid we can then write out an equation for the torque $\vec{\tau}_b$ applied by some potential $V(X^\alpha)$ on a base \mathcal{B}_b

$$\vec{\tau}_b = -\frac{\partial V(X^\alpha)}{\partial X^\alpha} \vec{\nabla}_b^r X^\alpha. \quad (\text{S24})$$

Here the torque is given in coordinates with respect to the lab frame (the reference frame in which the atomic

coordinates are provided by the MD engine). In order to have this torque act during an MD simulation it needs to be converted to a force for every atom i . The needed force can be found as follows

$$\vec{F}_i = m_i \vec{a}_i = m_i [\vec{r}_i \times \vec{\alpha}_b] = m_i \frac{\vec{r}_i \times \vec{\tau}_b}{I_b}. \quad (\text{S25})$$

Here \vec{r}_i is the vector pointing from the center of mass of the base \vec{r}_b^{com} to the position \vec{A}_i , of atom i $\vec{r}_i^{ff} = [\vec{A}_i - \vec{r}_b^{com}]^T$. Additionally I_b has been used to represent the moment of inertia of base with respect to the axis of the torque. Note that as the axis of the torque changes every time the constraint forces need to be calculated, so does I_b . Additionally I_b will change due to fluctuations within the base.

Aside from the rotations $\vec{\omega}$ and $\vec{\Omega}$ one might also want to impose some bias on the translations \vec{d} and \vec{D} . These are essentially the displacement between two rigid bodies expressed in the relevant midframe \mathbf{M} , and as such the gradients of these to atom position \vec{A}_i are

$$\vec{\nabla}_i d^\alpha = \pm \frac{m_i}{m_{base}} \mathbf{M}_{pair}[\alpha], \quad (\text{S26})$$

$$\vec{\nabla}_i D^\alpha = \pm \frac{m_i}{m_{pair}} \mathbf{M}_{step}[\alpha]. \quad (\text{S27})$$

Where the plus is used for the base above the step (noted ul and ur in the diagram of Fig. 2) and for the bases on the righthand strand (noted dr and ur in the diagram of Fig. 2) when considering \vec{D} and \vec{S} respectively.

Finally equations (S24) and (S25) can be combined with equations (S26), (S27) and (2) to give the final force on an atom i in base b (and thus in pair $p = b/2$ and steps $s = b/2$ and $s = b/2 - 1$) due to a potential on the collective variables $V(\vec{\omega}_p, \vec{\Omega}_s, \vec{d}_p, \vec{D}_s)$

$$\begin{aligned} \vec{F}_i = & - \sum_{\alpha} \frac{\partial V}{\partial \Omega_{\frac{b}{2}}^{\alpha}} \frac{m_i}{I_b} \left[\vec{r}_i \times \vec{\nabla}_b^r \Omega_{\frac{b}{2}}^{\alpha} \right] \\ & - \sum_{\alpha} \frac{\partial V}{\partial D_{\frac{b}{2}}^{\alpha}} \vec{\nabla}_i D_{\frac{b}{2}}^{\alpha} \\ & - \sum_{\alpha} \frac{\partial V}{\partial \omega_{\frac{b}{2}}^{\alpha}} \frac{m_i}{I_b} \left[\vec{r}_i \times \vec{\nabla}_b^r \omega_{\frac{b}{2}}^{\alpha} \right] \\ & - \sum_{\alpha} \frac{\partial V}{\partial d_{\frac{b}{2}}^{\alpha}} \vec{\nabla}_i d_{\frac{b}{2}}^{\alpha} \\ & - \sum_{\alpha} \frac{\partial V}{\partial \Omega_{\frac{b}{2}-1}^{\alpha}} \frac{m_i}{I_b} \left[\vec{r}_i \times \vec{\nabla}_b^r \Omega_{\frac{b}{2}-1}^{\alpha} \right] \\ & - \sum_{\alpha} \frac{\partial V}{\partial D_{\frac{b}{2}-1}^{\alpha}} \vec{\nabla}_i D_{\frac{b}{2}-1}^{\alpha}. \end{aligned} \quad (\text{S28})$$

For completeness we note that with respect to (2) we have replaced the exact positional gradients with versions that

apply rigid body dynamics. For translations they are replaced with gradients weighed to ensure all atoms in a base move together. For rotations we have substituted $\frac{m_i}{I_b} [\vec{r}_i \times \vec{\nabla}_b^r]$ for $\vec{\nabla}_i$. This last substitution is equivalent to projecting $\vec{\nabla}_i$ onto the plane normal to \vec{r} and again reweighing which ensures that constraint forces do not distort the internal structure of the bases.

S2. BIASING TWIST AND ROLL

To explain the response of the DNA under the effect of a bias in the twist and in the roll, we consider the following free energy model

$$f(\Omega_2, \Omega_3) = \frac{1}{2} \{ A_2 \Omega_2^2 + C \Omega_3^2 + 2G \Omega_2 \Omega_3 + K_r (\Omega_2 - \bar{\Omega}_2)^2 + K_t (\Omega_3 - \bar{\Omega}_3)^2 \} \quad (\text{S29})$$

with Ω_2 and Ω_3 excess roll and twist and A_2 , C and G the roll stiffness, the twist stiffness and the twist-roll coupling, respectively. Equation (S29) ignores higher order anharmonic terms which become important in the high deformation regime. The stiffnesses A_2 , C and G are sequence-dependent [1]. Here we consider the base pair step considered in Fig. 3, which is the central AT step of a DD sequence. The average excess roll and twist, $\langle \Omega_2 \rangle$ and $\langle \Omega_3 \rangle$ are obtained from the minimization of Eq. (S29).

We consider the two cases of a twist and roll bias. A twist bias corresponds to $K_r = 0$ and $K_t \neq 0$ in (S29). The minimum is obtained by setting the partial derivatives of the free energy f with respect to Ω_2 and Ω_3 to zero. In particular the condition $\partial f / \partial \Omega_2 = 0$ gives

$$\langle \Omega_3 \rangle = -\frac{A_2}{G} \langle \Omega_2 \rangle \quad (\text{S30})$$

In the case of a roll bias, corresponding to $K_r \neq 0$ and $K_t = 0$ in (S29), the condition $\partial f / \partial \Omega_3 = 0$ gives

$$\langle \Omega_3 \rangle = -\frac{G}{C} \langle \Omega_2 \rangle \quad (\text{S31})$$

Equations (S30) and (S31) give a linear dependence of $\langle \Omega_3 \rangle$ vs. $\langle \Omega_2 \rangle$. From prior work we know that $G > 0$ [28], which implies that $\langle \Omega_3 \rangle$ vs. $\langle \Omega_2 \rangle$ lines must have negative slopes. This is agreement with the simulation data of Fig. 3(b). Note that the two slopes are different, which is in agreement with (S30) and (S31). On average G is smaller than the two other couplings A_2 and C , which suggests a large slope for a twist bias (S30) and a small slope for a roll bias (S31), which is indeed observed in the simulation data of Fig. 3(b).